energies

Article

From Operations to Design: Probabilistic Day-Ahead Forecasting for Risk-Aware Storage Sizing in Wind-Dominated Power Systems

Dimitrios Zafirakis [1,*], Ioanna Smyrnioti [1], Christiana Papapostolou [2] and Konstantinos Moustris [3]

[1] Soft Energy Applications & Environmental Protection Laboratory, Mechanical Engineering Department, University of West Attica, 250 Thivon & P. Ralli Street, 12241 Athens, Greece; et04530@uniwa.gr
[2] Optimisation of Production Systems Laboratory, Department of Mechanical Engineering, University of West Attica, 250 Thivon & P. Ralli Street, 12241 Athens, Greece; chrispap@uniwa.gr
[3] Air Pollution Laboratory, Department of Mechanical Engineering, University of West Attica, 250 Thivon & P. Ralli Street, 12241 Athens, Greece; kmoustris@uniwa.gr
* Correspondence: dzaf@uniwa.gr; Tel.: +30-2105381580

Abstract

The large-scale integration of wind energy introduces increased uncertainty and variability in modern power systems, with direct implications for both system design and operation. In addressing similar aspects, energy storage plays a pivotal role as a key source of system flexibility. However, the design and sizing of storage systems remain challenging, especially under conditions of increased uncertainty. In this context, the present study proposes an alternative methodological framework, based on an inverse sizing pathway, i.e., from operations to design. More specifically, the uncertainty embedded in day-ahead forecasting of residual errors, associated with wind power generation and load demand, is currently exploited as a design-relevant signal, while energy storage is treated explicitly as a risk-hedging mechanism. Forecasting residuals spanning a year of operation are incorporated in the problem through probabilistic modeling, leading to the generation of trajectories that correspond to different risk levels and are managed as design scenarios. Regarding the modeling of uncertainties, the study examines two different strategies, namely a global modeling approach and a k-means clustering strategy. Accordingly, by mapping the interplay between storage capacity, uncertainty levels (or risk tolerance), achieved RES shares and system-level costs, we highlight the role of energy storage as a risk-hedging entity rather than merely a means of energy balancing. Our results to that end demonstrate that the achieved shares of RES exhibit increased sensitivity, even within constrained regions of wind power variation, while storage capacity features distinct zones of hedging value and hedging saturation effects emerging beyond certain storage levels. Moreover, evaluation of the two modeling strategies reflects on their complementary character, with the global modeling approach ensuring continuity and the clustering strategy capturing local asymmetries within different operational regimes. In conclusion, the methodology presented in this study bridges the gap between operational forecasting and long-term system design, offering a risk-aware framework for storage sizing, grounded in actual operational signals rather than relying on stationary historical data and relevant scenarios.

Keywords: probabilistic forecasting; artificial neural networks; wind energy; energy storage; risk hedging; risk management

Check for updates

Academic Editor: Marco Merlo

Received: 29 January 2026
Revised: 21 March 2026
Accepted: 16 April 2026
Published: 19 April 2026

Copyright: © 2026 by the authors. Licensee MDPI, Basel, Switzerland. This article is an open access article distributed under the terms and conditions of the Creative Commons Attribution (CC BY) license.

1. Introduction

The large-scale integration of renewable energy sources (RES) in modern power systems introduces a set of structural challenges, which are primarily associated with increased variability and uncertainty in power generation. These challenges may become more pronounced in wind-dominated systems, where large shares of power generation are determined by frequent and also intense short-term fluctuations, together with limited predictability. As a result, uncertainty in wind power generation entails direct implications for both the operational performance and the long-term design of such systems. Addressing similar challenges requires adequate system flexibility [1,2], which, amongst others, can be supported by the components of energy storage [3–6], demand side management [7–10], grid reinforcement [11], sector coupling [12] and advanced energy management [13]. Among these, energy storage plays a pivotal role by enabling balancing between variable wind energy generation and load demand, although at the expense of additional investment costs. At the same time, recent advancements in energy forecasting have led to substantial improvements regarding the short-term predictability of wind power generation, which reduces uncertainty at the operational level [14,15].

When combined, energy forecasting and energy storage operate as two complementary mechanisms for mitigating the impacts of wind power uncertainty, with forecasting reducing ex ante wind power uncertainty through improved predictions, and with storage providing ex post mitigation through the accommodation of wind energy variability and residual forecasting errors. Considering this, in the present study storage is perceived both as a means of addressing energy balance variability and as a mechanism for hedging uncertainties that determine wind-dominated power systems. Emphasis to that end is given on the second dimension and on the complementary roles and trade-offs between energy storage and energy forecasting [16–19].

In this context, the present study also places emphasis on the design of wind-dominated power systems and, in particular, on the risk-aware sizing of energy storage in similar settings. In contrast to conventional methods of energy planning—where either deterministic approaches [20–22] or probabilistic modeling, both relying solely on historical data [23], are employed—we adopt an alternative design strategy, grounded in operational uncertainty. In more detail, we currently exploit day-ahead, hourly forecasting residuals of wind power generation [24] and load demand [25] over a year's period and treat these as design-relevant uncertainty signals. Toward this direction, uncertainties are integrated into the problem through the adoption of a probabilistic modeling framework and the resulting probabilistic trajectories are interpreted as scenarios of long-term planning determined by different levels of risk tolerance. This, essentially, introduces a conceptual shift, i.e., rather than restricting probabilistic forecasts to operational hedging, we embed the relevant uncertainties in the design stage explicitly, challenging the conventional practice of distinguishing system operation from system planning.

As a result, the adopted methodological framework aims to link short-term operational forecasting with long-term system design, enabling storage sizing decisions that account for the assumption of different levels of operational risk. This redefines the focus of storage planning from resource variability to operational forecasting uncertainty, enabling storage to be interpreted as a risk-hedging asset against forecast errors rather than solely as a buffer for energy imbalances, thereby challenging the standard baseline of historical, scenario-based sizing through the introduction of a risk-hedging design philosophy and the proposition of an inverse sizing pathway, i.e., from operations to design. In the same context, our approach treats forecasting as part of a closed loop [26], linking prediction, system operation, and design outcomes. This means that forecasting performance is currently evaluated on the basis of system-level indicators [27,28] rather than conventional accuracy

metrics [29]. In more detail, through the probabilistic propagation of forecasting residuals to long-term design outcomes, the joint impact of wind power and load demand uncertainties is determined against the required levels of storage capacity for risk-hedging [30], bounded by the resulting RES shares and LCOE at the system level. Under this perspective, the value of forecasting models is eventually assessed in terms of their ability to limit operational risk and reduce additional flexibility requirements and overall system costs, thereby associating forecasting performance with long-term system design.

The remainder of this paper is structured as follows. Section 2 introduces the methodological framework, presenting input data of the research and describing the architecture of the forecasting models developed. Accordingly, in Section 3 we present the results of our research, drawing from the application of two distinct probabilistic modeling strategies and putting emphasis on mapping the impact of forecasting uncertainties on key system-level indicators, i.e., achieved RES shares and levelized cost of energy (LCOE), across the entire problem space. Next, Section 3 proceeds with a risk-aware storage sizing exercise, for which we constrain the examined problem space into a set of meaningful scenarios, and concludes with the conduction of a sensitivity analysis focusing on the variation of key cost parameters. Finally, Section 4 discusses the key findings of the analysis and critically reviews the limitations of the proposed approach, providing at the same time the main conclusions of our research.

2. Data and Methodology

2.1. Methodological Framework

The proposed methodological framework is summarized in the block diagram in Figure 1. Initially, forecasting models based on artificial neural networks (ANNs) are developed for day-ahead (DA), hourly predictions of wind power capacity factor (CF) and load demand. Wind power CF and load demand stand as the two uncertainty components of the research, informing the probabilistic approach currently adopted. In more detail, following the designation of optimal ANN architectures [24,25], baseline forecasts and forecast residuals are generated. These comprise the basis for the formulation of the probabilistic problem, which in turn investigates two different strategies concerning the modeling of residuals' distributions, i.e., global modeling and k-means clustering [31].

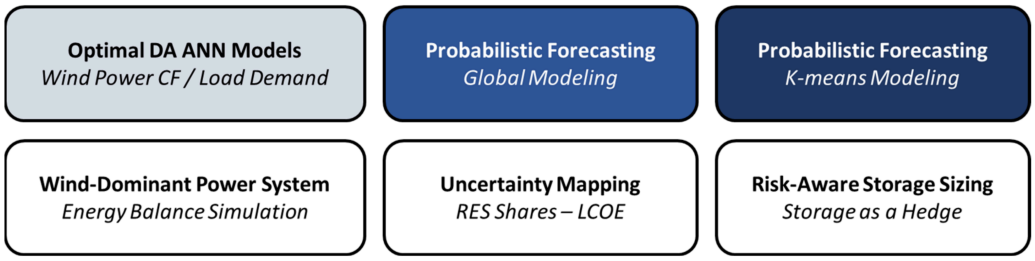

Figure 1. Methodological framework block diagram.

Probabilistic scenarios are shaped on the basis of applying different percentiles that call upon the modeled residual distributions, subsequently enabling probabilistic-driven energy balance simulations for the system under investigation. To that end, a first-order energy balance simulation analysis is conducted on an hourly basis, assuming a wind power-dominant system, supported primarily by energy storage, and secondly by oil-based generation as back-up. Aiming to isolate the impact of forecasting uncertainty on wind power generation and load demand, the simplified simulation approach currently adopted focuses on energy balance, and not on unit commitment aspects. Therefore, it does not explicitly incorporate certain operational constraints such as system-level constraints (e.g.,

technical minima, start-up/shut-down times and ramping limitations of the conventional oil-based power units, as well as dynamic penetration limits affecting the dispatchability of wind energy) and storage-related constraints (e.g., ramping limitations of the storage asset).

Concerning the application of the probabilistic approach, different percentile scenarios are applied consistently across consecutive days, rather than exhaustively, i.e., exploring all possible inter-day combinations. This offers a meaningful risk spectrum, within which we put forward a risk-aware sizing exercise for the storage component. In this context, we treat storage as a risk-hedging entity and proceed with assessing storage capacity requirements and their sensitivity in supporting guaranteed bands of annual RES shares under different levels of risk tolerance. At the same time, obtained results are projected onto the estimation of system-level LCOE, thus allowing for a broader economic evaluation of the problem in hand.

2.2. Input Data and Forecasting Models

Following the outline of the methodological framework, in the current section we present the problem's input data and detail the architecture of optimal ANN models used, leveraging previous research of the authors [24,25]. Regarding wind power, the dataset used consisted of hourly theoretical CF values covering a full year (2019), with multiple model architectures tested so as to predict the 24 h CF values of rolling days-ahead.

Concerning the training process of the model, we used time series from 2019 and developed two subsets of data. The first subset included 80% of the available training dataset, with the remaining 20% constituting the second subset used for the purpose of cross-validation. The subsets were created randomly, while, for the performance evaluation of the models, we exploited data series from 2020 not used in the training stage of the models. For load demand, a richer dataset covering a 2.75-year period (1 January 2016–30 September 2018) was employed, representing the demand profile of a small-scale island system. Training and validation followed the same procedural steps, while performance evaluation was carried out against data from 2019. Of the models tested, the optimal wind power CF model corresponds to a Generalized Feedforward Neural Network (GFNN) with 38 input neurons, 2 hidden layers of 35 and 17 neurons respectively, and a single output neuron (Figure 2). Training was based on gradient descent with momentum, and the activation function applied was tanhaxon. The optimal load demand model on the other hand was a multilayer perceptron (MLP) with 28 input neurons, a single hidden layer of 50 neurons, and a single output neuron (Figure 3), also employing the back-propagation algorithm and the tanhaxon activation function.

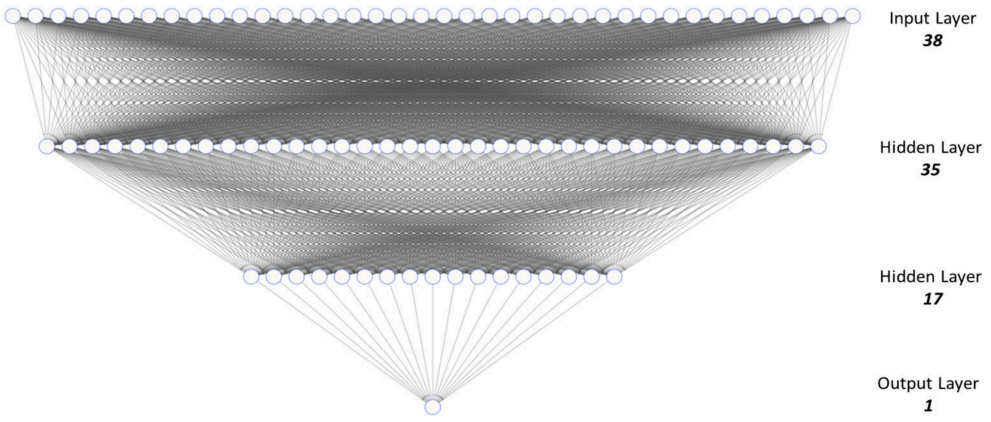

Figure 2. Architecture of the wind power CF ANN forecasting model.

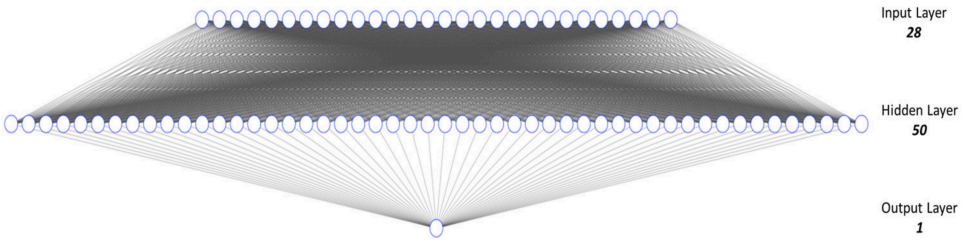

Figure 3. Architecture of the load demand ANN forecasting model.

The input features for each model are listed in Tables 1 and 2, while the statistical performance metrics are summarized in Table 3. Performance was measured using the correlation coefficient (R), the mean bias error (MBE), the root mean square error (RMSE), and the index of agreement (IA). To that end, the GFNN wind power CF model exhibits moderate predictive ability, whereas the MLP load demand model is found to demonstrate stronger performance.

Table 1. Input (training) data and output target—wind power CF forecasting model.

Input (Training)	Output (Target)
The month number (1–12) for 1, 2, 3, 4, and 5 days before The day number (1–31) for 1, 2, 3, 4, and 5 days before The hour (H) of the day (1–24) for 1, 2, 3, 4, and 5 days before The absolute maximum value of the CF index within the 12 hours preceding the forecast hour (H), for each of the 5 previous days The absolute minimum value of the CF index within the 12 hours preceding the forecast hour (H), for each of the 5 previous days The theoretical value of the CF index for the corresponding hour (H), for 1, 2, 3, 4, and 5 days before the forecast day The actual value of the CF index for the corresponding hour (H), for 1, 2, 3, 4, and 5 days before The month number (1–12) on the next forecast day (D + 1) The day number (1–31) on the next forecast day (D + 1) The hour (H) of the day (1–24) on the next forecast day (D + 1)	The hourly theoretical value of CF for hour (H) on the next forecast day (D + 1)

Table 2. Input (training) data and output target—load demand forecasting model.

Input (Training)	Output (Target)
The month number (1–12) for 1, 2, 3, 4, and 5 days before The day number (1–31) for 1, 2, 3, 4, and 5 days before The hour (H) of the day (1–24) for 1, 2, 3, 4, and 5 days before Air temperature (°C) for each hour (H) for the 5 previous days Load demand (kW) for each hour (H) for the 5 previous days Month number (1–12) for the prediction day (D + 1) Day number (1–31) for the prediction day (D + 1) Hour (1–24) for the prediction day (D + 1)	The hourly value of load demand for hour (H) on the next forecast day (D + 1)

Table 3. Statistical metrics—optimal wind power CF and load demand forecasting models.

Model	R	MBE	RMSE	IA
GFNN	0.516	−0.030	0.230	0.695
MLP	0.952	2.388 kW	44.453 kW	0.975

This is better illustrated in Figure 4, where time series of observed and predicted values are plotted for the entire period of examination. As can be seen, the wind power CF model, although reproducing medium-range values of CF effectively, is found to underperform in the lower and upper extremes (Figure 4a). On the other hand, the load demand model (Figure 4b) appears consistent in almost the entire range of the load profile spectrum, with the exception of distinctively low values of load demand across the year.

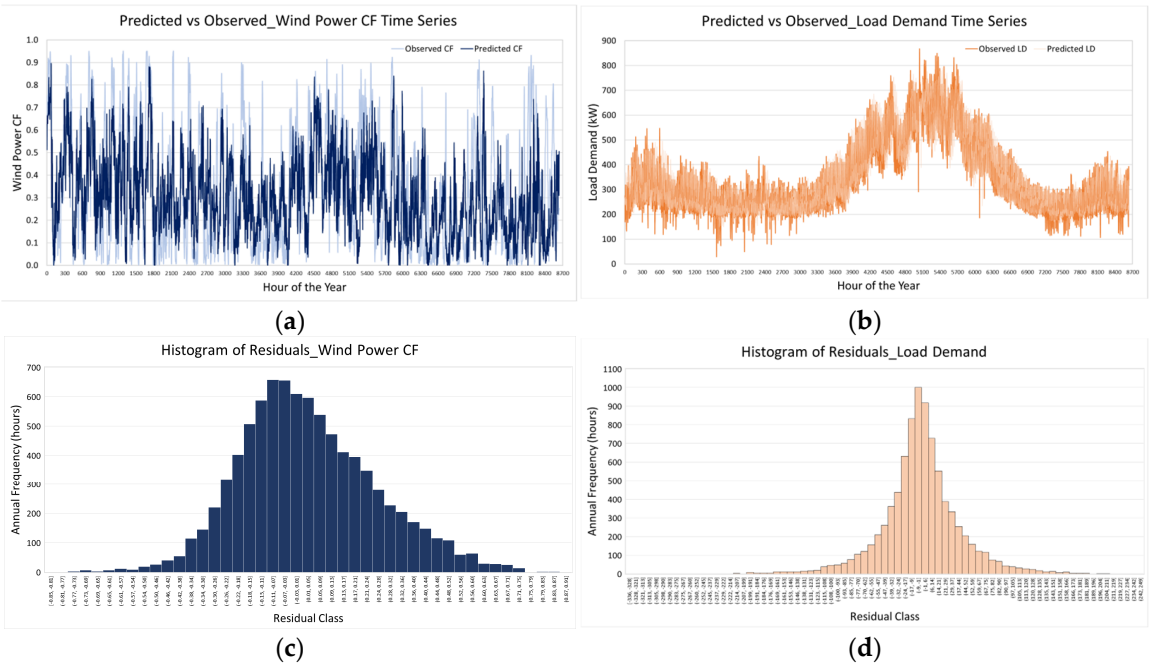

Figure 4. Observed vs. predicted wind power CF (**a**) and load demand (**b**), and residual histograms of wind power CF (**c**) and load demand (**d**) forecasting models.

Another way to interpret the performance of the given models is through the respective residual distributions, provided in Figure 4c,d. According to the histograms, wind power CF presents a right-skewed distribution (average residual of ~−0.03 and standard deviation of 0.228), while load demand approximates a normal distribution, determined by an average residual of −2.19 kW and a standard deviation of ~44 kW. Overall, it can be argued that the load demand model achieves high predictive accuracy while the wind power CF model exhibits greater uncertainty, especially over the tails of the distribution. Accordingly, this asymmetry between the two models becomes inherent in the development of probabilistic scenarios and the calibration of deterministic forecasting through the percentile-based incorporation of residuals, as this is further analyzed in Section 3 of the paper.

3. Application Results

3.1. Probabilistic Forecasting

Following the presentation and performance evaluation of the two forecasting models, in this section we proceed with the probabilistic calibration of the corresponding wind power CF and load demand predictions. This is achieved through the systematic integration of forecasting residuals into the baseline predictions provided by the models. Toward this direction, we employ two different modeling strategies, which are projected on the inverse cumulative distributions of forecasting residuals (Figure 5) for both wind power CF and load demand.

Namely, these correspond to a global modeling strategy, in which we model the entire range of residuals under a single model equation, and to a clustering strategy, in which we use the k-means method for the determination of residual clusters, which are next modeled separately. In this context, the first approach presents the advantage of relying on a more informative, robust dataset, leveraging data continuity, while the second approach provides a more targeted representation of forecast uncertainty per different data regions, on the basis however of less populated datasets per cluster.

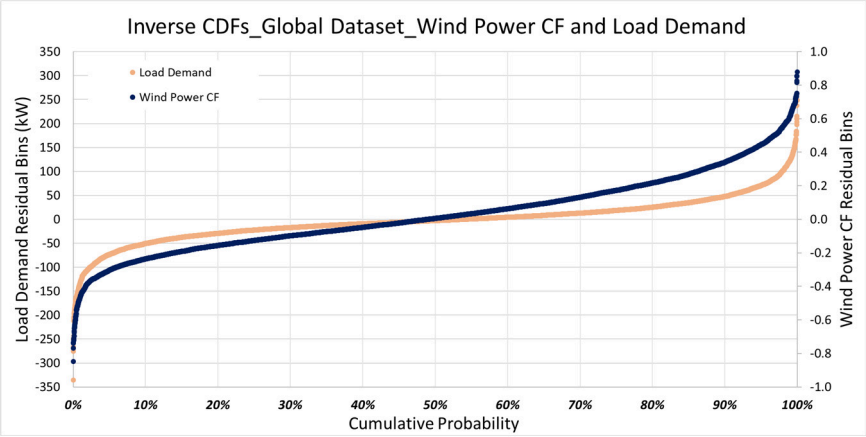

Figure 5. Inverse cumulative distributions of wind power CF and load demand residuals.

3.1.1. Global Modeling Strategy

As has already been seen, with the global modeling strategy, we capture the entire range of the inverse cumulative probability curves given in Figure 5, and determine best-fit polynomials for the wind power CF and load demand components. The respective seventh-order polynomials are provided in Table 4, with $R(p)$ formulas returning the residuals' value under the application of percentiles p, across all prediction points obtained.

Table 4. Global modeling strategy—wind power CF and load demand best-fit polynomials (The polynomial coefficients presented in Tables 4–6 have been rounded for the purpose of readability).

Component	Best-Fit Polynomial	R^2
Wind CF	$R(p)_{wind} = -0.534 + 6.535p - 52.764p^2 + 234.851p^3 - 572.775p^4 + 773.250p^5 - 541.186p^6 + 153.310p^7$	0.997
Load Demand	$R(p)_{load} = -159.368 + 2484.721p - 20{,}806.688p^2 + 92{,}719.994p^3 - 226{,}945.862p^4 + 307{,}084.792p^5 - 215{,}177.010p^6 + 60{,}946.462p^7$	0.986

Table 5. Clustering modeling strategy—wind power CF best-fit polynomials.

Predicted Wind CF	Best-Fit Polynomial	R^2
0–0.1035	$R(p)_{wind} = 30.593p^7 - 92.647p^6 + 110.606p^5 - 66.027p^4 + 21.700p^3 - 4.075p^2 + 0.724p - 0.092$	0.9989
0.1035–0.1955	$R(p)_{wind} = 52.608p^7 - 177.951p^6 + 239.485p^5 - 162.023p^4 + 58.562p^3 - 10.987p^2 + 1.215p - 0.190$	0.9992
0.1955–0.2849	$R(p)_{wind} = 21.328p^7 - 74.4567p^6 + 108.368p^5 - 82.217p^4 + 34.110p^3 - 7.374p^2 + 1.122p - 0.274$	0.9994
0.2849–0.3796	$R(p)_{wind} = 45.299p^7 - 151.188p^6 + 205.616p^5 - 145.804p^4 + 57.067p^3 - 11.631p^2 + 1.592p - 0.364$	0.9999
0.3796–0.4842	$R(p)_{wind} = 14.282p^7 - 35.062p^6 + 31.462p^5 - 13.568p^4 + 4.451p^3 - 1.861p^2 + 1.284p - 0.441$	0.9996
0.4842–0.6147	$R(p)_{wind} = -26.619p^7 + 93.983p^6 - 127.873p^5 + 83.844p^4 - 25.780p^3 + 1.599p^2 + 1.836p - 0.565$	0.9991
>0.6147	$R(p)_{wind} = 13.420p^7 - 66.9796p^6 + 139.982p^5 - 156.567p^4 + 100.756p^3 - 37.625p^2 + 8.143p - 0.850$	0.9946

Table 6. Clustering modeling strategy—load demand best-fit polynomials.

Predicted Load (kW)	Best-Fit Polynomial	R^2
100–238.376	$R(p)_{load} = 42{,}924.2p^7 - 150{,}313.2p^6 + 214{,}366.4p^5 - 160{,}018.4p^4 + 67{,}063.1p^3 - 15{,}749.1p^2 + 1990.7p - 126.0$	0.9943
238.376–296.303	$R(p)_{load} = 55{,}068.1p^7 - 196{,}046.4p^6 + 282{,}174.3p^5 - 210{,}306.1p^4 + 86{,}527.4p^3 - 19{,}456.8p^2 + 2295.9p - 144.1$	0.9920
296.303–369.086	$R(p)_{load} = 50{,}681.2p^7 - 184{,}199.3p^6 + 271{,}439.8p^5 - 207{,}916.6p^4 + 88{,}348.8p^3 - 20{,}624.8p^2 + 2534.0p - 163.4$	0.9901
369.086–453.037	$R(p)_{load} = 65{,}348.3p^7 - 227{,}155.0p^6 + 316{,}722.6p^5 - 226{,}310.1p^4 + 87{,}999.7p^3 - 18{,}310.4p^2 + 1977.8p - 128.4$	0.9682
453.037–545.333	$R(p)_{load} = 39{,}194.0p^7 - 136{,}073.0p^6 + 191{,}813.7p^5 - 141{,}020.8p^4 + 58{,}033.9p^3 - 13{,}369.7p^2 + 1737.2p - 146.2$	0.9971
545.333–643.884	$R(p)_{load} = 88{,}982.2p^7 - 322{,}124.1p^6 + 472{,}575.2p^5 - 360{,}218.0p^4 + 152{,}147.1p^3 - 35{,}106.8p^2 + 4184.7p - 250.0$	0.9916
>643.884	$R(p)_{load} = 57{,}474.1p^7 - 205{,}074.7p^6 + 295{,}284.9p^5 - 219{,}451.5p^4 + 89{,}680.1p^3 - 20{,}001.2p^2 + 2{,}467.8p - 208.9$	0.9962

Correlation between actual and modeled residuals is illustrated in the plots in Figure 6, where global models appear to perform efficiently overall, with the exception however of distribution tails, over which both best-fit polynomials become less adequate. This indicates that the models properly capture the central distribution of residuals, but underperform in the representation of extreme residuals, which, on the other hand, correspond to low-probability events that carry a limited contribution over the entire distribution.

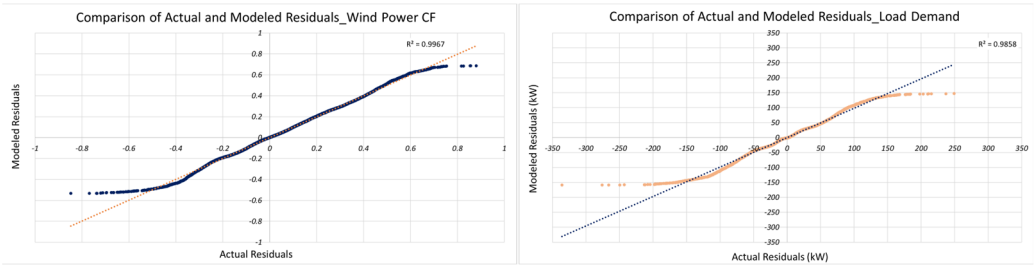

(**a**) (**b**)

Figure 6. Actual vs. modeled residuals for the wind power CF (**a**) and load demand (**b**) components.

Applying the best-fit global polynomials for different percentiles leads to the development of probabilistic scenarios spanning the entire range of cumulative probability. Such an indicative instance is provided in Figure 7, reflecting probabilistic forecasting results for a time span of 20 consecutive days, i.e., from hour 480 to hour 960 of the year. In more detail, three sub-instances are illustrated, which present the probabilistic variation in wind power CF, load demand and anticipated state of charge (SoC) for storage.

For each case, cumulative probability levels are shown, expressed as percentiles from p_0 to p_{100}, with the respective trajectories illustrating the range of possible outcomes around the point of forecast, overlaid with the predicted and observed time series. Results obtained highlight the higher uncertainty attributed to wind power CF in comparison to load demand, which is due to the performance of forecasting models and the inherently higher variability in wind power regimes. The impact of load uncertainty alone is then projected onto storage cycling.

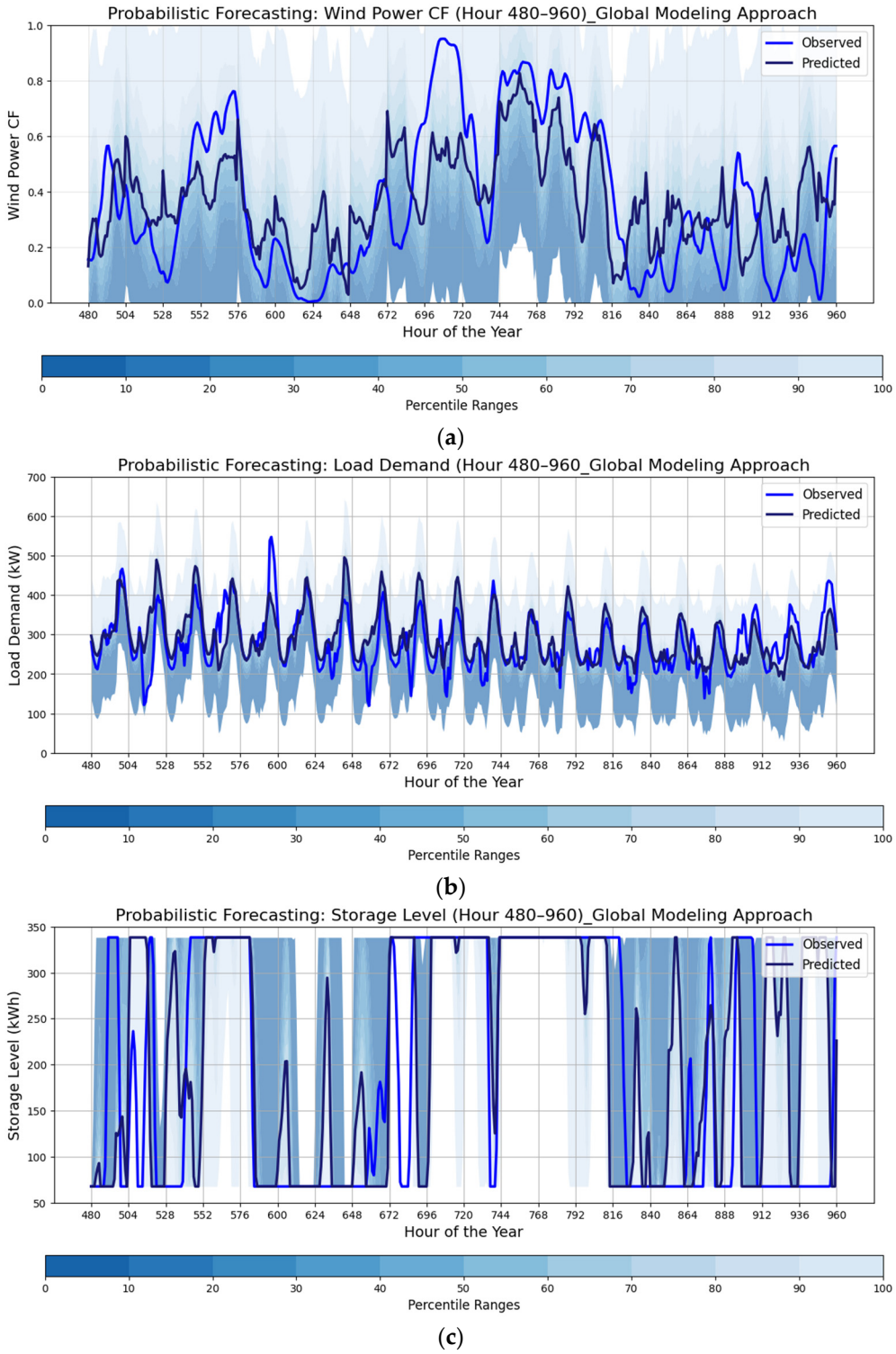

Figure 7. Probabilistic forecasting instances: wind power CF (**a**), load demand (**b**), storage SoC (**c**).

To that end, a relatively tight storage with a capacity equivalent to 1 h against the annual average load demand of the examined system (~340 kWh) is currently tested, given a fixed p_{50} wind power CF trajectory and a fixed wind capacity of 100% against the system's annual peak load demand. As expected, each of the probabilistic trajectories of load demand introduces different residual balances and therefore different charging and discharging requirements for the storage asset, with SoC profiles found to diverge considerably, even under the integration of the least uncertain problem dimension, i.e., load demand. In more detail, lower load demand percentiles reduce stress on storage

and higher ones lead to deeper cycling and more frequent storage depletion. This in turn carries implications for the capacity of storage to act as a risk-hedging asset, dedicated to guaranteeing achieved RES shares within predefined bands.

Finally, and with regard to the long-term impact of employing different percentiles, it must be mentioned that the selection of percentiles below and above certain thresholds introduces significant bias (e.g., for wind power CF, for $p \leq p_{30}$, the long-term CF drops below ~21%, while for $p \geq p_{70}$, it exceeds 43%, compared to the observed mean of 33% and the predicted one of 30%).

This underlines the fact that the attempted transition from operations to design and the associated risk interpretation of probabilistic results must remain bounded within certain meaningful limits of the problem space. On top of that, and focusing on the modeling approach, it should also be mentioned that under the global modeling strategy, uncertainty is assumed to be symmetrically distributed over different prediction points, providing a more uniform canvas that enhances continuity but lacks a more conditional error allocation.

3.1.2. Clustering Modeling Strategy

To further explore the sensitivity of design outcomes against an alternative approach of uncertainty modeling, the clustering of prediction points was implemented as a second modeling strategy. This enables targeted residual modeling and weighted calibration of predictions under different wind power CF and load demand regimes within the broader problem space.

For that purpose, the k-means clustering algorithm was applied in order to distinguish prediction regimes into meaningful clusters. By following an empirical analysis based on the elbow method, the designated number of clusters for both wind power CF and load demand predictions was selected equal to 7, with the analysis yielding marginal-only difference in intra-cluster variance around that point, revealing a saturation pattern for additional clusters.

The corresponding clusters' boundaries regarding predicted values and the relevant best-fit polynomials (seventh-order polynomials) are provided in Tables 5 and 6 for the wind power CF and load demand components respectively, while in Figure 8, the inverse cumulative probability distributions of residuals per designated prediction cluster are also given. Accordingly, the probabilistic forecasting instances presented earlier under the global modeling approach are reproduced under the application of the clustering-based approach, with results obtained given in Figure 9.

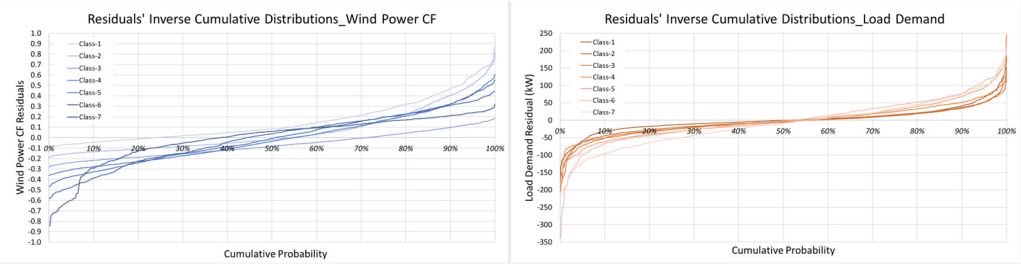

(**a**) (**b**)

Figure 8. Inverse CDFs of wind power CF (**a**) and load demand (**b**)—clustering strategy.

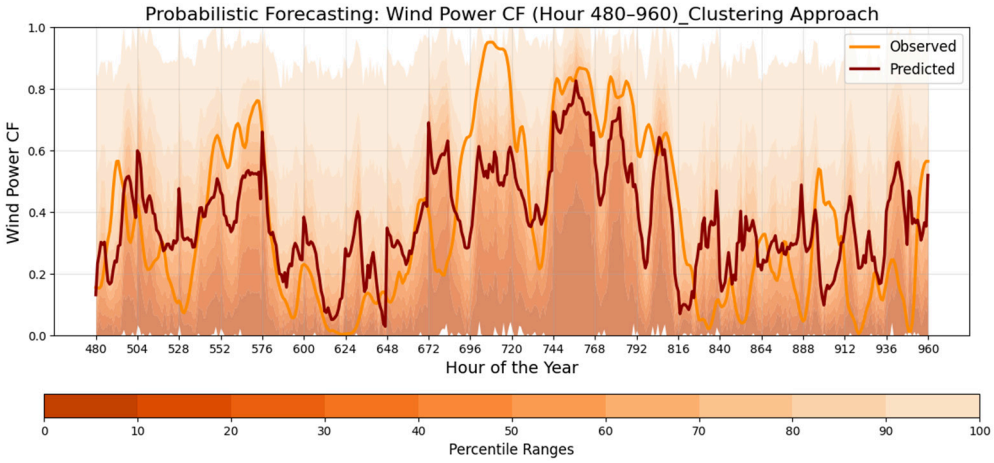

(**a**)

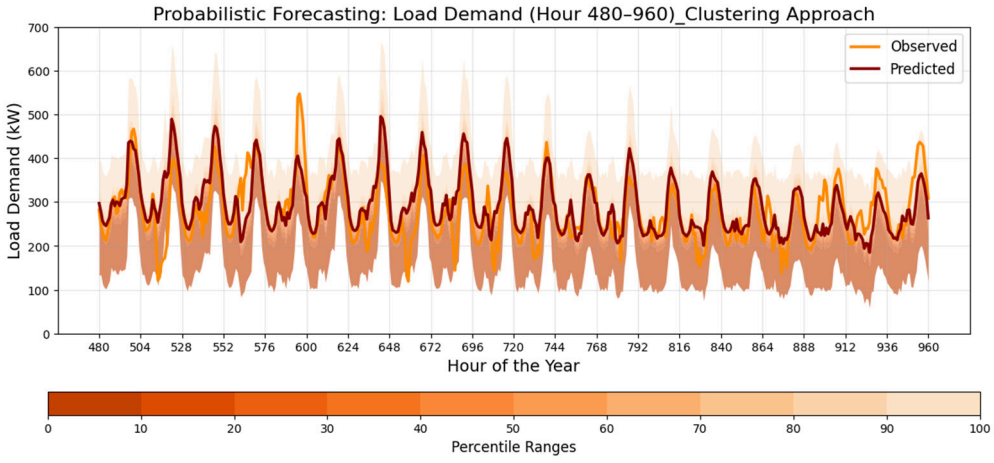

(**b**)

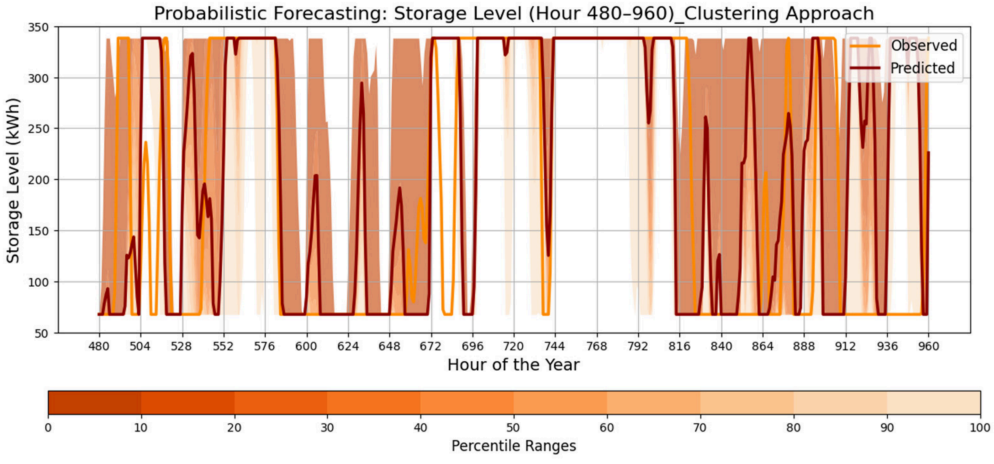

(**c**)

Figure 9. Probabilistic forecasting instances: wind power CF (**a**), load demand (**b**), storage SoC (**c**).

As can be seen in the plots, the clustering-based approach induces a more asymmetric error allocation across different prediction regimes, which becomes particularly pronounced in the higher and lower extremes of the anticipated wind power CF. For the higher-end wind power CF cluster, calibrated results appear more constrained, while the opposite is true for the lower-end cluster, where lower-percentile trajectories expand closer to zero CF values. This behavior is consistent with the heterogeneity of polynomial coefficients across the different prediction clusters (see also Table 5) and highlights the impact of local error allocation in capturing different risk levels for different prediction regimes. To that end,

these differences further influence the operational behavior of the storage configuration through more localized variations in cycling intensity, opposite to the smoother transition dynamics expected in the case of the global modeling strategy.

3.2. Guaranteed RES Shares and System-Level LCOE

Following the presentation of probabilistic forecasting instances under the application of the two different modeling strategies adopted, in the current section we proceed with a mapping exercise, examining the interplay of assumed storage capacity and integrated uncertainties of wind power CF and load demand on two key design indicators, i.e., achieved annual RES shares and system-level LCOE. In this context, we treat storage as a risk-hedging asset, associating risk interpretation with the ability of the system to assimilate different levels of uncertainty while achieving and maintaining guaranteed RES shares within predefined bands of constrained variation. To that end, we let storage capacity vary from 0 to 10 h of equivalent storage duration and monitor the shift in the levels of integrated uncertainty under different RES share targets. Results are subsequently extended to the estimation of the system LCOE, where the trade-off between storage capacity and risk assimilation is also evaluated in economic terms. In support of that, the cost assumptions underpinning the LCOE calculation are given in Table 7, while two sets of plots are presented for each modeling strategy examined (Figures 10 and 11).

Table 7. Cost parameters for the estimation of system-level LCOE.

Cost Parameter	Assigned Value	Unit
Wind CAPEX	2000	€/kW
Wind Power Capacity	100%	over system peak demand
Storage CAPEX	750	€/kWh
Balance of System Costs	10%	over system CAPEX
Price of Oil	1.1	€/lt
Annual Maintenance Factor	3%	over system CAPEX
Diesel Efficiency	30%	
Oil Calorific Value	10	kWh/lt
Annual Discount Rate	5%	-
Investment Horizon	20	Years

In each set of plots, load demand percentiles vary from p_0 to p_{100}, while the corresponding wind power CF percentiles shift dynamically, following the increase in RES shares within the assumed RES bands. Additionally, for each p_{CF}, the relevant variation in p_{LD} is illustrated through boxplots, while storage capacity points are superimposed to indicate the variation in required storage capacity across different uncertainty spaces. Each load demand percentile plot is further paired with a corresponding LCOE plot against the same mapping space. In this context, Figure 10 gathers the pairs of plots for the global modeling strategy. Three different pairs of plots are presented, corresponding to different RES bands ranging between 50 and 60%, 60% and 70%, and lastly 70–80%. At this point, it should be mentioned that the achieved RES shares under the deterministic approach (application of observed wind power CF and load demand values) and the application of prediction signals (baseline predictions of wind power CF and load demand values) yields RES shares that range between ~61.3–65.7% and ~64.5–68.2%.

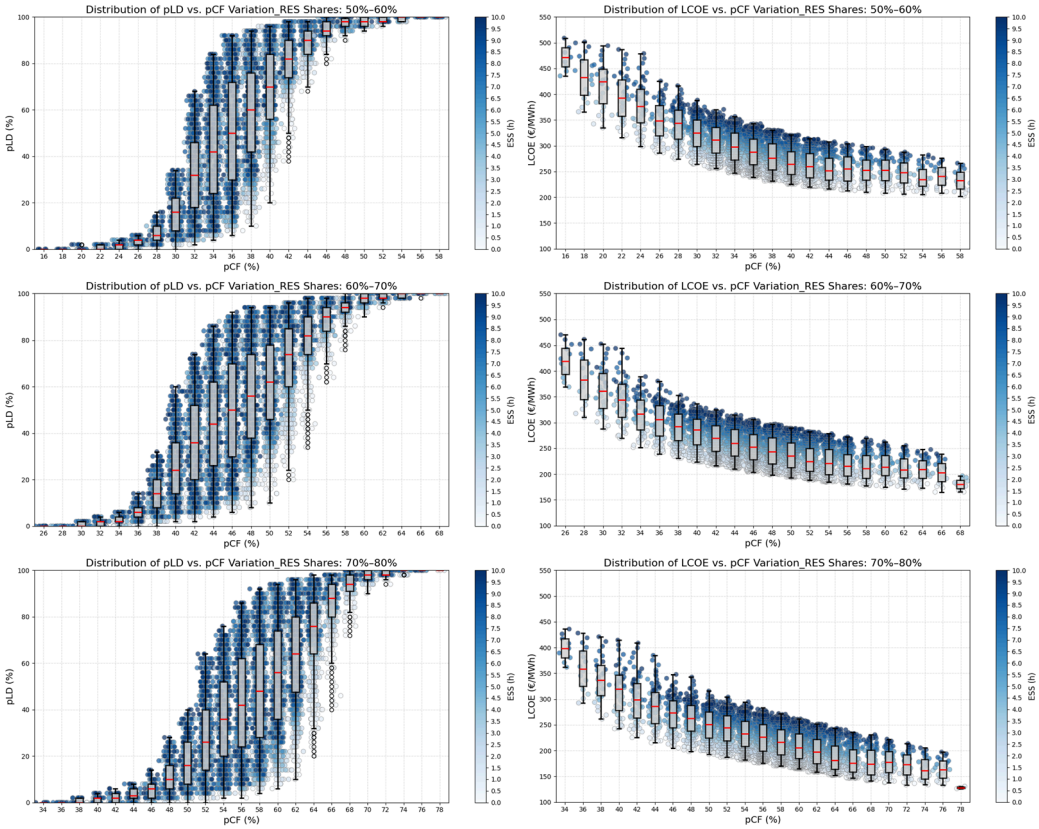

Figure 10. Mapping the impact of uncertainties under the global modeling strategy.

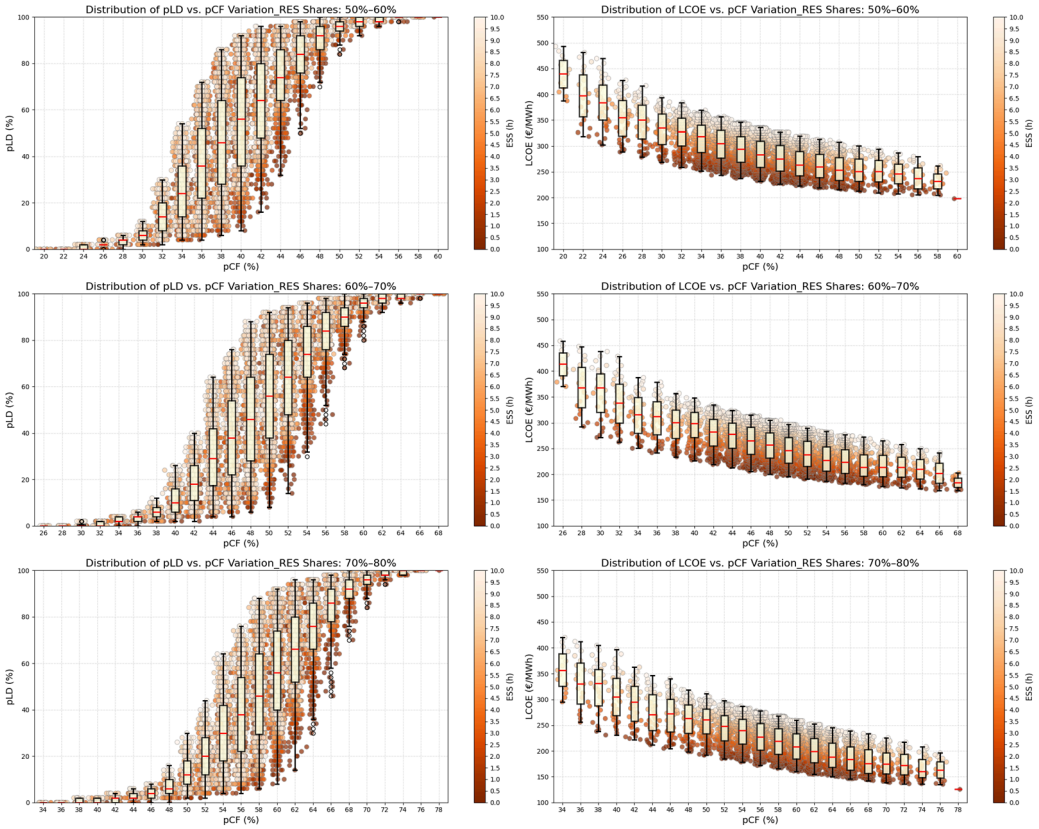

Figure 11. Mapping the impact of uncertainties under the clustering modeling strategy.

Under the given bands of guaranteed RES shares, a gradual shift can be noted in Figure 10 towards higher percentiles of wind power CF, in the ranges of p_{16}–p_{58}, p_{26}–p_{68} and p_{34}–p_{78}, with fixed wind power CF percentiles absorbing lower percentiles of load demand as guaranteed RES shares are set to increase. At the same time, variation in storage capacity, operating as a hedging entity, offers the potential for the assimilation of risk associated with the application of higher load demand percentiles. These ranges tend to expand for mid-range percentiles of wind power CF, designating the more significant impact of storage in this area, and become thinner over the tails of the S-shaped distributions where sub-distributions (per bin of wind power CF percentile) become less populated in terms of available points, and the influence of storage capacity fades. An inverse behavior is noted for the LCOE indicator. In more detail, an increase in wind power CF percentiles signals a notable overall reduction that may even exceed 250–300 €/MWh, while, the internal variation in LCOE, per sub-distribution, yields LCOE differences that exceed 100 €/MWh for the low and mid-range wind power CF percentiles, reflecting the variation in storage capacity and load demand percentiles.

Shifting to the next set of plots (Figure 11) regarding the application of the clustering modeling strategy, the results obtained expose an expansion of wind power CF percentiles to higher values for the lower RES band of 50–60%. Moreover, median boxplot values of load demand percentiles per wind power CF slice imply lower tolerance with regard to the risk that can be assimilated under the overall range of the storage capacity examined. This appears predominantly over lower and mid-range wind power CF percentiles, maximizing for the lower RES band of 50–60% (~10%) and gradually diminishing with the increase in RES shares examined. Furthermore, LCOE plots present a similar pattern, with results obtained demonstrating slight increases in LCOE under the k-means modeling approach, mainly for mid-range wind power CF percentiles and for RES shares below 70%.

3.3. Risk-Aware Storage Sizing

Following the initial mapping exercise, in the given section we focus on the role of storage as a risk-hedging asset within a more constrained space of uncertainty, combining both modeling strategies applied. To that end, we provide a more targeted estimation of storage capacity requirements in order to offset the risk of load demand and wind power variation, in response to the prerequisite of meeting certain bands of RES shares on an annual basis. In doing so, we isolate local distributions of load demand percentiles attached to different wind power CF trajectories (percentiles) and examine four different inter-variation bands, i.e., 50–60%, 60–70%, 70–80% and 80–90%. For each of the bands we estimate the mean storage capacity under the application of both modeling strategies applied and also provide the associated system-level LCOE, while monitoring the variation in RES shares within the predefined bands.

Results of the analysis are given in Figures 12–14, where mean storage capacity, RES shares and LCOE are plotted across a constrained space of wind power CF percentiles, i.e., from p_{30} to p_{70}, with each curve representing a different band of RES shares and with continuous and dashed lines referring to the global and the clustering modeling strategy respectively. The p_{CF} window selected is considered sufficiently wide to capture meaningful operational forecasting risk and narrow enough to avoid drifting into extreme-year representations. In the examined system, the interval of p_{30} to p_{70} corresponds to implied annual CF values of ~21–43%, against an observed mean of 33%, thus defining a wide yet operationally interpretable uncertainty envelope that aligns with empirical evidence on the variation in wind power CF for a given wind power installation [32]. At this point, it is important to note that given the medium–high wind potential of the area currently examined, the anticipated wind power CF can be quite sensitive to small deviations in average wind

speed, owing to high operational frequency concentrated around the transitional segment of a typical wind power curve. This suggests that the magnitude of variation for the wind power CF, deriving from the relevant forecast residuals, may justify the percentile window applied. Overall, it can be argued that narrower ranges may fail to capture the problem sensitivity sufficiently, whereas broader ones may increasingly risk an overlap between forecast-driven uncertainty and extreme-year representation.

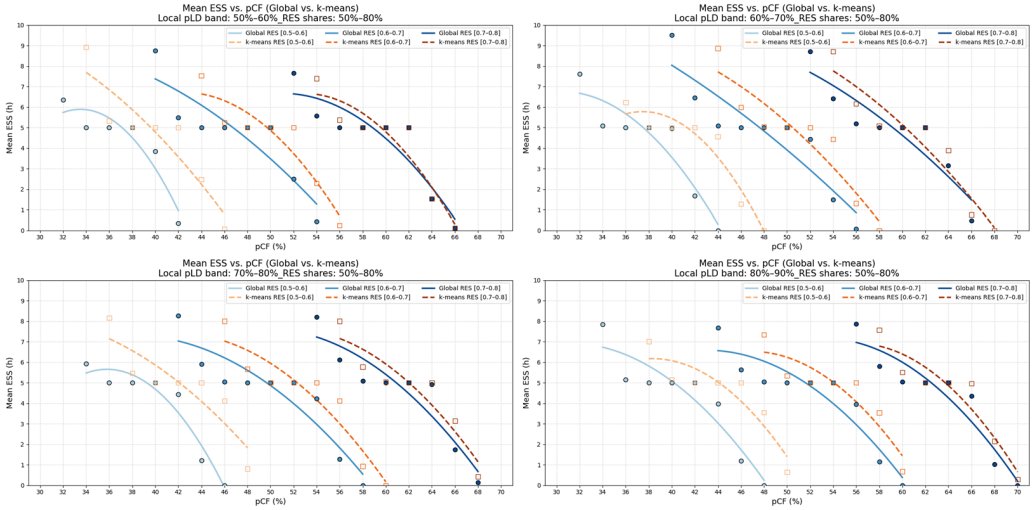

Figure 12. Mean storage capacity per local p_{LD} and different RES bands, against the variation in p_{CF}.

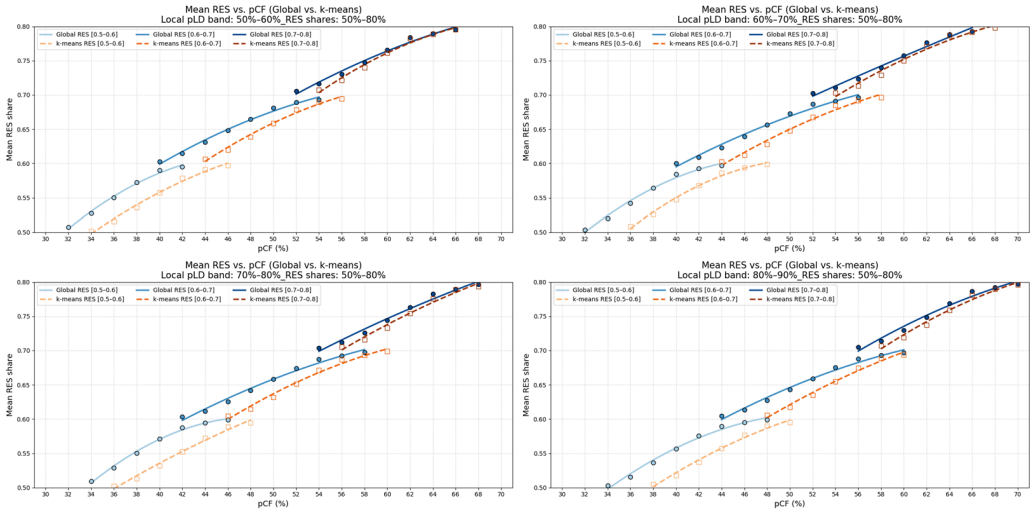

Figure 13. RES shares per local p_{LD} and different RES bands, against the variation in p_{CF}.

To that end, a first key finding of the analysis (Figure 12) suggests that storage requirements decrease intensively with the increase in p_{CF}, designating wind power availability as the primary source of uncertainty against which storage provides a compensating mechanism. At the same time, the challenge of meeting higher load demand levels (sequence of plots) also generates an impact, which is regime-dependent and strongly affected by wind power CF percentiles. In particular, higher load conditions lead to a relative increase in storage requirements, especially for the lower p_{CF} tails. Furthermore, across all mean storage capacity plots, a storage saturation zone is identified, which in this case lies around 5 h, effectively absorbing a broad range of load and wind power uncertainty.

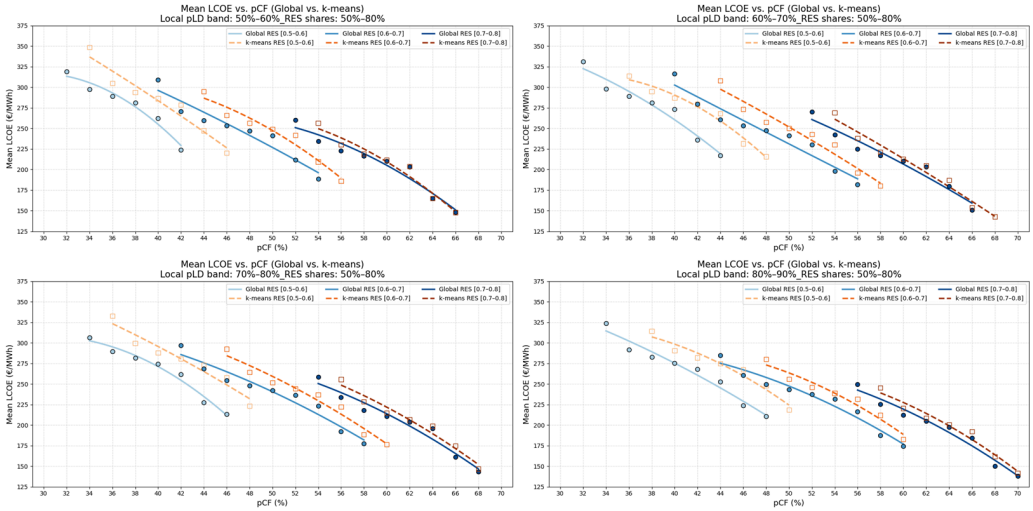

Figure 14. Mean LCOE per local p_{LD} and different RES bands, against the variation in p_{CF}.

The above are consistent with the variation in RES shares given in Figure 13. In general, intra-curve increases in wind power CF correspond to increments of 10% in RES penetration, which aligns with the predefined RES shares' classes. Additionally, it can be seen that to maintain a given RES share under higher local p_{LD} bands requires a shift to higher wind power CF percentiles (two wind power CF percentile units in most cases). Moreover, and concerning the impact of local p_{LD} variation for a certain p_{CF} percentile, although designated in Figures 10 and 11, it is currently obscured by the increase in storage capacity; e.g., in the 80–90% p_{LD} band and at $p_{CF} = p_{48}$, the slight increase in RES shares from ~60% to ~63% suggests an increase of 5 h in storage. To that end, while both storage needs and RES shares are predominantly driven by wind power uncertainty, it should also be noted that local, load-related risk also exerts a secondary, less-trackable influence.

The previous outputs next propagate on LCOE results (Figure 14), with a decrease in storage capacity (Figure 12) and an increase in RES shares (Figure 13) leading to a significant decrease in LCOE. This is primarily driven by storage and emerges more emphatically for storage capacities falling below the identified saturation zone. The cost of risk hedging is thus mainly determined by the additional storage capacity required to compensate for reduced wind availability at lower p_{CF} values, and is further amplified under higher-load-demand conditions. Along a given curve, this effect is reflected in substantial LCOE spreads, with differences between the tails even reaching ~100 €/MWh.

Overall, by observing the entire set of plots, it can be seen that the transition across RES classes within a given plot (i.e., for overlapping curves under common values of p_{CF}) reflects the intra-curve effect of increasing RES shares, requiring approximately ~3.5–4.0 h of additional storage capacity per class and leading to a corresponding increase of 20–30 €/MWh in LCOE. At the same time, the comparison across different plots reflects the inter-curve effect of rising load demand, leading to systematic increases in storage requirements and resulting in LCOE increases in the order of 10–25 €/MWh across the examined p_{LD} range. In conclusion, storage capacity acts as a hedging mechanism against the risk introduced by the two uncertainty components. Under adverse conditions, i.e., low p_{CF} values or high p_{LD} values, additional storage capacity mitigates the risk of failing to meet RES targets, at the expense however of an associated cost.

Results obtained also indicate distinct regimes of storage capacity with regard to hedging effectiveness and relevant value. For modest storage capacities ($\leq$2 h), an entry-level hedging potential can be observed, where storage acts as a limited buffer against small deviations, enabling marginal compliance with the desired RES targets. The main

hedging zone accordingly emerges in the range of 2 h to 5 h. It is in this given zone that the expansion of storage allows the accommodation of substantially more adverse conditions of p_{CF} and p_{LD}, at the cost however of higher costs (LCOE) driven by storage. Beyond this range, saturation behavior is noticed, with diminishing marginal hedging value owing to considerably higher storage costs. Finally, a comparison between the global and the k-means modeling strategies reveals consistent trends against the variation in uncertainty components, with systematic differences in the magnitude of the estimated indicators. In more detail, the k-means modeling strategy yields higher storage requirements and LCOE, while generating lower RES shares, especially in low-p_{CF} and lower-RES regimes. These differences seem to diminish as RES shares increase, with both strategies eventually converging in areas of higher RES bands.

3.4. Sensitivity Analysis

In this section, we evaluate the impact exerted by the variation in key cost parameters on the resulting, system-level LCOE, using a subset of solutions identified previously (local p_{LD} band of 60–70%). Additionally, we also compare two k-mean configurations, corresponding to different numbers of clusters (baseline scenario of k = 7 and k = 5) (Figure 15). Regarding cost assumptions, we examine an increase in oil price, from 1.1 €/lt to 1.5 €/lt, and a reduction in turnkey capital costs for the wind and storage components (from 2000 €/kW to 1500 €/kW and from 750 €/kWh to 250 €/kWh, respectively).

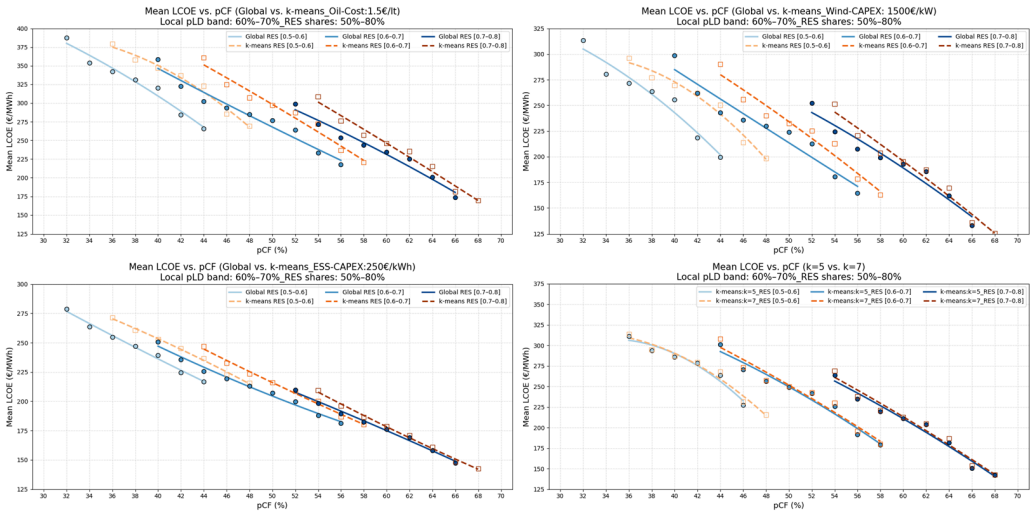

Figure 15. Mean LCOE sensitivity analysis, following the variation in key cost parameters and k-means configurations.

As expected, the increase in oil price (~36%) signals a rise in LCOE, which is proportional to the system's reliance on oil-based power generation, and thus is inversely related to the RES shares achieved. This effect is observed across the entire p_{CF} range, with lower values of p_{CF} exhibiting increases of up to ~50 €/MWh, and with higher ones presenting a more moderate increase of ~25 €/MWh (global approach), owing to higher RES shares achieved. On the other hand, the k-means modeling approach demonstrates slightly higher sensitivity, which diminishes with the increase in p_{CF} (see also Figure 13).

Conversely, a 25% reduction in wind capital costs results in an approximately uniform decrease in LCOE of 25 €/MWh across the entire p_{CF} range, holding no noticeable difference between the two modeling approaches. A more pronounced effect is observed for the examined reduction in the capital cost of storage (~67%), entailing decreases in LCOE that exceed 50 €/MWh at low values of p_{CF}, gradually declining to ~25 €/MWh at higher p_{CF}

values, owing to reduced storage requirements. At the same time, differences between the two modeling approaches diminish, with the corresponding curves converging closely.

Finally, the comparison between k = 5 and k = 7 confirms the robustness of the baseline clustering choice (k = 7), since the resulting LCOE curves are almost identical, indicating negligible sensitivity between the two configurations.

4. Discussion and Conclusions

The current study followed a deliberate, inverse methodological pathway from operations to design, interpreting the inherent uncertainty in wind power and load demand forecasting as a means of expressing different levels of risk tolerance in the design of wind-dominated power systems. In this context, storage was treated as a risk-hedging asset, capable of absorbing the combined uncertainty of wind power and load demand forecasts, with our results quantifying the impact induced on key design indicators, i.e., achieved RES shares and system-level LCOE. These indicators were then used as signals and targets in order to inform a comprehensive mapping exercise on risk-aware storage sizing.

To that end, we employed two different modeling strategies so as to integrate forecasting residuals, namely a global and a clustering modeling strategy, which allowed for a more holistic assessment of the problem sensitivity across an additional dimension of uncertainty representation. The global approach, relying on the assumption of stationary residuals, supported continuity and symmetry in the distribution of uncertainties, leading to a more homogeneous allocation of forecast risk across operating regimes. Contrariwise, the clustering-based approach introduced a more asymmetric, weighted allocation of risk. Keeping that in mind, it must be noted that the two strategies should be perceived as complementary rather than competing, with the global approach offering a continuous baseline upon which the clustering strategy unfolds signals and behaviors of local character, allowing for a more systematic exploration of the problem space.

Moreover, and as has already been seen, the application results obtained designated different zones of hedging value and relevant cost associating with the role of storage as a hedge across the examined uncertainty space. Risk absorption and hedging value to that end intensified in the range of 2 h to 5 h of storage capacity against the average hourly load demand of ~340 kWh, which, to relate with the features of the given power system, corresponds to a peak-to-average ratio of ~2.5 for the load demand component, and to a wind power-to-peak load demand ratio of 100%.

This 5 h limit also indicated a saturation zone concerning planning implications [28]. Within it, storage achieved hedging over a wide risk space, shaped by both the wind power CF and the load demand component, thus designating its value as a risk-hedging mechanism. Beyond it, however, the marginal value of storage diminished, since the resulting system costs presented a notable increase. This highlights the potential of storage to act as a risk-hedging mechanism in similar, wind-dominated configurations, under rational storage capacity, as well as the fact that beyond a given saturation zone, the development of flexibility portfolios, such as with the introduction of demand side management and sector coupling [9,12], should also be explored to avoid extreme system costs.

Another important aspect concerns the sensitivity of the identified storage hedge zone to the quality of the forecasting models used to generate the uncertainty signals. Since the main uncertainty driver refers to the wind power CF forecast residuals, obtaining a more accurate wind power CF forecasting model would most likely lead to a narrower uncertainty envelope, reducing storage capacity requirements against the baseline of a less efficient model. Conversely, a less accurate wind power CF model would imply greater uncertainty, and therefore, the need for higher hedging capabilities and storage capacities. Arguably, this is reflective of the complementary roles of forecasting accuracy and energy

storage capacity in the optimization of modern power systems, also highlighting the urgency to advance energy forecasting on the one hand and reduce storage and flexibility costs on the other.

Regarding modeling assumptions of the study, it should be mentioned that our modeling approach considered a first-order energy balance simulation, neglecting unit commitment constraints such as technical minima, ramping times and also the dynamic RES penetration limit at the system level. The incorporation of such constraints would on the one hand increase the likelihood of wind energy curtailments, thereby enhancing the value of storage as a flexibility resource, and on the other highlight the importance of integral flexibility for storage assets through, e.g., the need for higher power-to-capacity ratios in order to accommodate faster response requirements. Furthermore, the assumption of persistent percentiles across consecutive days constrained the risk assessment space and the broader operational dynamics of the system examined, allowing however for a more regulated mapping of associated risks.

Overall, the results obtained indicate that the problem of storage design is not merely an optimization problem, but should also be treated as a problem of risk tolerance. In this context, the value of storage relies on its hedging potential to mitigate the impact of uncertainties upon the goal to achieve guaranteed RES shares and not solely on its potential to allow for a more competitive system in purely economic terms. To conclude, the methodology presented aimed to bridge the gap between operational forecasting and long-term system design, offering a framework of risk-aware storage sizing based on actual operational signals, rather than stationary historical data and scenarios.

Author Contributions: Conceptualization, D.Z. and I.S.; methodology, D.Z. and C.P.; software, D.Z. and K.M.; validation, C.P. and I.S.; data curation, I.S. and D.Z.; writing—original draft preparation, D.Z. and I.S.; writing—review and editing, C.P. and K.M.; visualization, D.Z. and I.S.; supervision, C.P., K.M. and D.Z. All authors have read and agreed to the published version of the manuscript.

Funding: This research received no external funding.

Data Availability Statement: Wind data were retrieved from the open database MERRA-2, through the online tool Renewables.ninja—https://www.renewables.ninja (accessed on 10 March 2023—in the context of previous research [24]) and load demand data were provided by the Hellenic Electricity Distribution Network Operator, also in the context of previous research conducted by the authors [25].

Acknowledgments: Results of this research expand on the undergraduate thesis of Smyrnioti, conducted during her studies in the Mechanical Engineering Department of the University of West Attica.

Conflicts of Interest: The authors declare no conflicts of interest.

References

1. Lund, P.D.; Lindgren, J.; Mikkola, J.; Salpakari, J. Review of energy system flexibility measures to enable high levels of variable renewable electricity. *Renew. Sustain. Energy Rev.* **2015**, *45*, 785–807. [CrossRef]
2. Khalili, S.; Lopez, G.; Breyer, C. Role and trends of flexibility options in 100% renewable energy system analyses towards the Power-to-X Economy. *Renew. Sustain. Energy Rev.* **2025**, *212*, 115383. [CrossRef]
3. Conde, H.J.C.; Demition, C.M.; Honra, J. Storage is the New Black: A Review of Energy Storage System Applications to Resolve Intermittency in Renewable Energy Systems. *Energies* **2025**, *18*, 354. [CrossRef]
4. Mahadevan, V.; Raja, S.; Ali Rusho, M.; Yishak, S. Critical review of energy storage systems: A comparative assessment of mechanisms, advantages, challenges, and integration with renewable energy. *Results Eng.* **2025**, *26*, 105589. [CrossRef]
5. Elalfy, D.A.; Gouda, E.; Kotb, M.F.; Bureš, V.; Sedhom, B.E. Comprehensive review of energy storage systems technologies, objectives, challenges, and future trends. *Energy Strategy Rev.* **2024**, *54*, 101482. [CrossRef]
6. De Carne, G.; Maroufi, S.M.; Beiranvand, H.; De Angelis, V.; D'Arco, S.; Gevorgian, V.; Waczowicz, S.; Mather, B.; Liserre, M.; Hagenmeyer, V. The role of energy storage systems for a secure energy supply: A comprehensive review of system needs and technology solutions. *Electr. Power Syst. Res.* **2024**, *236*, 110963. [CrossRef]

7. El-Araby, E.E.; Yorino, N. A demand side response scheme for enhancing power system security in the presence of wind power. *Int. J. Electr. Power Energy Syst.* **2023**, *146*, 108714. [CrossRef]
8. Devine, M.T.; Nolan, S.; Lynch, M.A.; O'Malley, M. The effect of Demand Response and wind generation on electricity investment and operation. *Sustain. Energy Grids Netw.* **2019**, *17*, 100190. [CrossRef]
9. Zafirakis, D.; Christopoulos, K.; Moustris, K.; Kaldellis, J.K. Stochastic Assessment of Day-Ahead, Wind Energy Curtailment-Driven Demand Response Requirements in Non-Interconnected Island Systems. *Environ. Sci. Proc.* **2023**, *26*, 176.
10. Rao, C.K.; Sahoo, S.K.; Padhan, S. Advanced Optimization Approaches for Demand Side Management in Renewable Energy Generation System. *Unconv. Resour.* **2026**, *11*, 100302. [CrossRef]
11. ACER. Electricity Infrastructure Development to Support a Competitive and Sustainable Energy System. 2025. Available online: https://www.acer.europa.eu/sites/default/files/documents/Publications/ACER_2024_Monitoring_Electricity_Infrastructure.pdf (accessed on 12 April 2026).
12. Gea-Bermúdez, J.; Jensen, I.G.; Münster, M.; Koivisto, M.; Kirkerud, J.G.; Chen, Y.; Ravn, H. The role of sector coupling in the green transition: A least-cost energy system development in Northern-central Europe towards 2050. *Appl. Energy* **2021**, *289*, 116685. [CrossRef]
13. Azeroual, M.; Moughraoui, F.Z.; El Lysaouy, L.; ELMarkhi, H. Intelligent energy management for wind-integrated microgrids using multi-agent systems. *Wind. Eng.* **2026**. [CrossRef]
14. Benti, N.E.; Chaka, M.D.; Semie, A.G. Forecasting Renewable Energy Generation with Machine Learning and Deep Learning: Current Advances and Future Prospects. *Sustainability* **2023**, *15*, 7087. [CrossRef]
15. Haq, I.U.; Kumar, A.; Rathore, P.S. Machine learning approaches for wind power forecasting: A comprehensive review. *Discov. Appl. Sci.* **2025**, *7*, 1139. [CrossRef]
16. Emde, A.; Märkle, L.; Kratzer, B.; Schnell, F.; Baur, L.; Sauer, A. Effects of Load Forecast Deviation on the Specification of Energy Storage Systems. *Designs* **2023**, *7*, 107. [CrossRef]
17. Bitaraf, H.; Rahman, S.; Pipattanasomporn, M. Sizing Energy Storage to Mitigate Wind Power Forecast Error Impacts by Signal Processing Techniques. *IEEE Trans. Sustain. Energy* **2015**, *6*, 1457–1465. [CrossRef]
18. Yu, X.; Dong, X.; Pang, S.; Zhou, L.; Zang, H. Energy Storage Sizing Optimization and Sensitivity Analysis Based on Wind Power Forecast Error Compensation. *Energies* **2019**, *12*, 4755. [CrossRef]
19. Li, Z.; Xiang, Y.; Liu, J. Forecasting error-aware optimal dispatch of wind-storage integrated power systems: A soft-actor-critic deep reinforcement learning approach. *Energy* **2025**, *318*, 134798. [CrossRef]
20. Kaldellis, J.K. Optimum autonomous wind–power system sizing for remote consumers, using long-term wind speed data. *Appl. Energy* **2002**, *71*, 215–233. [CrossRef]
21. Kapsali, M.; Anagnostopoulos, J.S.; Kaldellis, J.K. Wind powered pumped-hydro storage systems for remote islands: A complete sensitivity analysis based on economic perspectives. *Appl. Energy* **2012**, *99*, 430–444. [CrossRef]
22. Katsaprakakis, D.A.; Christakis, D.G.; Pavlopoylos, K.; Stamataki, S.; Dimitrelou, I.; Stefanakis, I.; Spanos, P. Introduction of a wind powered pumped storage system in the isolated insular power system of Karpathos–Kasos. *Appl. Energy* **2012**, *97*, 38–48. [CrossRef]
23. Kaldellis, J.K.; Kapsali, M.; Tiligadas, D. Presentation of a stochastic model estimating the wind energy contribution in remote island electrical networks. *Appl. Energy* **2012**, *97*, 68–76. [CrossRef]
24. Moustris, K.; Zafirakis, D. Day-Ahead Forecasting of the Theoretical and Actual Wind Power Generation in Energy-Constrained Island Systems. *Energies* **2023**, *16*, 4562. [CrossRef]
25. Moustris, K.; Kavadias, K.A.; Zafirakis, D.; Kaldellis, J.K. Medium, short and very short-term prognosis of load demand for the Greek Island of Tilos using artificial neural networks and human thermal comfort-discomfort biometeorological data. *Renew. Energy* **2020**, *147*, 100–109. [CrossRef]
26. Zhang, H.; Li, R.; Chen, Y.; Chu, Z.; Sun, M.; Teng, F. Risk-aware objective-based forecasting in inertia management. *arXiv* **2023**, arXiv:2303.11785. [CrossRef]
27. Davis, D.; Brear, M.J. Impact of short-term wind forecast accuracy on the performance of decarbonising wholesale electricity markets. *Energy Econ.* **2024**, *130*, 107304. [CrossRef]
28. Yan, J.; Li, X.; Wang, H.; Si, F.; Qiao, W.; Liu, Y. The economic value of wind power forecasting: A data-driven method and its application in various scenarios. *Energy* **2025**, *340*, 139151. [CrossRef]
29. Koutsandreas, D.; Spiliotis, E.; Petropoulos, F.; Assimakopoulos, V. On the selection of forecasting accuracy measures. *J. Oper. Res. Soc.* **2022**, *73*, 937–954. [CrossRef]
30. Haessig, P.; Multon, B.; Ben Ahmed, H.; Lascaud, S.; Bondon, P. Energy storage sizing for wind power: Impact of the autocorrelation of day-ahead forecast errors. *Wind. Energy* **2015**, *18*, 43–57. [CrossRef]

31. Rathod, D.; Gidwani, L. A literature review based on density forecasting and uncertainty quantification of wind power generation. *Renew. Sustain. Energy Rev.* **2026**, *229*, 116559. [CrossRef]
32. Solbrekke, I.M.; Kvamstø, N.G.; Sorteberg, A. Mitigation of offshore wind power intermittency by interconnection of production sites. *Wind. Energy Sci.* **2020**, *5*, 1663–1678. [CrossRef]

Disclaimer/Publisher's Note: The statements, opinions and data contained in all publications are solely those of the individual author(s) and contributor(s) and not of MDPI and/or the editor(s). MDPI and/or the editor(s) disclaim responsibility for any injury to people or property resulting from any ideas, methods, instructions or products referred to in the content.